Hysteretic transition between states of a filled hexagonal magnetic dipole cluster

Andrew D. P. Smith,[1] Peter T. Haugen,[2] and Boyd F. Edwards[2]
[1)]*St. John's College, University of Cambridge, Cambridge CB2 1TP, UK*
[2)]*Department of Physics, Utah State University, Logan, Utah 84322, USA*

By minimizing the magnetostatic potential energy and by finding zeros in the sum of the squares of the torques, we find the equilibrium states of six dipoles of identical strength at the vertices of a regular hexagon and a variable-strength dipole at the center. The seven dipoles spin freely about fixed axes that are perpendicular to the plane of the hexagon, with their dipole moments directed parallel to the plane. When the central dipole is weak compared with the perimeter dipoles, a "circular" state applies in which the perimeter dipole moments circle around the central dipole, which points toward a perimeter dipole. When the central dipole is strong, a more symmetric "dipolar" state applies in which the perimeter dipole moments align approximately with the field of the central dipole. Over an intermediate range of dipole strengths bounded by two critical values, both states are locally stable and the state of the system depends upon its history. Iron filings are used to observe both states in experiments on small spherical neodymium magnets. A "misaligned" state that is barely unstable theoretically is also observed experimentally; this state resembles the circular state except that the central dipole moment points toward a point of contact between two perimeter magnets.

I. INTRODUCTION

Collections of small neodymium magnet spheres are popular desk toys that are used to build beautiful sculptures, thanks to the angular dependence of the dipole interaction.[1] These collections also serve as pedagogical tools for demonstrating principles of mathematics, physics, chemistry, biology, and engineering.[2]

These magnets have spherically symmetric dipole distributions, so their magnetic interactions match those of two point dipoles.[3–5] This equivalence simplifies investigations of magnet chain, ring, and tube formation,[6–8] magnet chain energy,[9] mechanical properties of chains and cylinders,[10] chain pattern formation,[11] stable defects along chains and rings,[12] eigenmodes for lateral oscillations of a straight chain,[13] stability of vertical chains,[14] magnetic crystal formation,[15] stability of magnetic rings with a central dipole directed out of the plane,[16] radiation damping for two magnets oscillating in each other's fields,[17] the motion of a dipole that slides freely along the surface of a fixed dipole,[18] the dynamics of a free dipole that bounces elastically against a fixed dipole,[19,20] the motion of two dipoles that slide freely against each other,[21] and the normal modes for dipoles whose rotation axes are fixed at the vertices of a regular polygon.[22]

In this paper, we illustrate how a simple dipole system can exhibit complex nonlinear behavior. We explore the equilibrium states of a system of seven dipoles, with six identical perimeter dipoles located at the vertices of a regular hexagon and one dipole of variable strength at the center, forming a "filled hexagon" (Fig. 1). The relative strength of the central dipole $\alpha = m_0/m$ is the ratio of the magnitudes of the magnetic moments of the central and perimeter dipoles. The filled hexagon with $\alpha = 1$ serves as a building block for many sculptures made from collections of small neodymium magnets.[1]

The positions of the seven dipoles are fixed and the dipoles are allowed to spin freely about axes that are perpendicular to the plane of the hexagon, with their magnetic moments confined to this plane. We calculate equilibrium dipole orientations as a function of α by minimizing the magnetostatic potential energy and by finding zeros in the sum of the squares of the torques on the seven dipoles. We test the stability of equilibrium states by examining the eigenvalues and the determinant of the Hessian of the potential energy.

We also observe equilibrium states experimen-

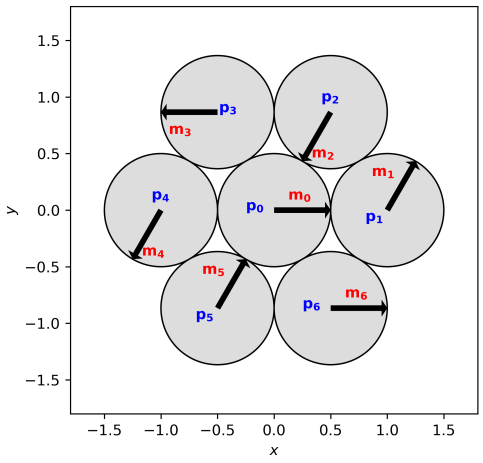

FIG. 1. Illustration of the positions $\mathbf{p_0}$...$\mathbf{p_6}$ and dipole moments $\mathbf{m_0}$...$\mathbf{m_6}$ of seven dipoles confined to the $x-y$ plane. The seven dipoles are free to rotate about fixed axes in the z direction.

tally by photographing patterns of iron filings on a piece of paper resting on a filled hexagon of seven nickel-plated neodymium magnet spheres of diameter 5 mm. In these observations, we use magnets of two different strengths but of the same size: commercially available fully-magnetized "strong" magnets and partially magnetized "weak" magnets obtained from the same manufacturer.[23] These magnets enable observations for $\alpha = 0$ (using six strong magnets in the perimeter and no magnet at the center), $\alpha = 0.42$ (using a weak magnet at the center and six strong magnets in the perimeter), $\alpha = 1$ (using strong magnets for all seven magnets), and $\alpha = 2.4$ (using a strong magnet at the center and six weak magnets in the perimeter).

In the lowest-energy "circular" state for $\alpha = 1$, the six perimeter dipole moments circle around the central dipole, whose moment points toward the center of a perimeter dipole [Fig. 2(a)]. This state is stable theoretically and is observed in our experiments [Fig. 2(b)]. The circular state is predicted to be stable for $\alpha < \alpha_2 = 2.47$, above which it no longer exists.

With an energy that is barely larger than the circular state for $\alpha = 1$, the "misaligned" state resembles the circular state except that the central dipole moment points not toward a perimeter dipole, but toward the gap between two perimeter dipoles [Fig. 2(c)]. This equilibrium state is unstable theoretically for all α, is barely unstable for $\alpha = 1$, and is observed in our $\alpha = 1$ experiments with about the same frequency as the circular state [Fig. 2(d)]. Our calculations ignore friction between magnets, which is present in our experiments.

The "dipolar" state has the third-lowest energy at $\alpha = 1$. This state is unstable and unobservable at this value of α, but is predicted to be stable for $\alpha > \alpha_1 = 1.15$. In this state, the six perimeter dipoles align approximately with the field of the central dipole and the central dipole moment points toward the center of a perimeter dipole. Figures 2(e) and (f) show this state theoretically and experimentally for $\alpha = 2.4$. As $\alpha \to \infty$, the perimeter dipoles are predicted to align exactly with the field of the central dipole.

The circular, misaligned, and dipolar states have planes of reflection symmetry that are perpendicular to the magnetic moment of the center dipole. In Figs. 2(b), (d), and (f), these planes are indicated by green dotted lines. The dipolar state also has a time-reversed reflection symmetry (a reflection followed by a time reversal) that is indicated in Fig. 2(f) by blue dashed lines.

The circular and misaligned states show approximate pentagonal symmetries that honor their reflection symmetries, with five clumps of iron filings located approximately at the vertices of a regular pentagon [Fig. 2(b), (d)]. This curious symmetry contrasts with the underlying hexagonal symmetry of the magnet positions and helped to motivate this study. Experimentally, it is easy to distinguish between the circular and misaligned states. In the circular state, the plane of reflection symmetry passes through points of contact between perimeter magnets [Fig. 2(b)]. In the misaligned state, the plane of reflection symmetry passes through the centers of perimeter magnets [Fig. 2(d)]. As $\alpha \to 0$, the circular and misaligned states reduce to the equilibrium state of a hexagon ring, with all six dipoles pointing tangent to a circle.[22]

The system is predicted to exhibit hysteresis as α varies because the circular and dipolar states are

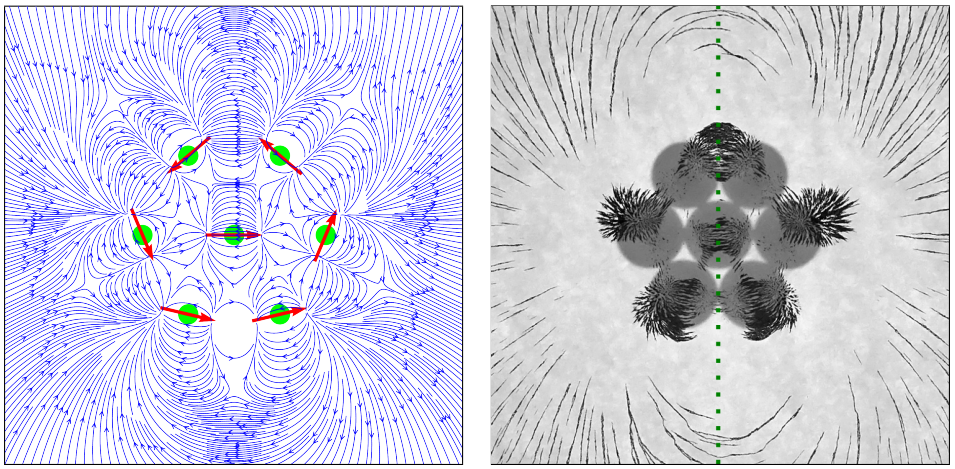

(a) $\alpha = 1$ circular state, fields

(b) $\alpha = 1$ circular state, filings

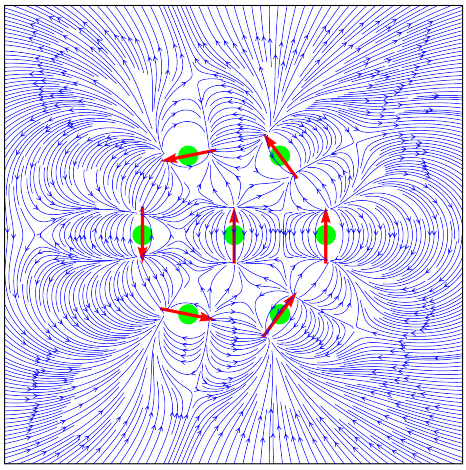

(c) $\alpha = 1$ misaligned state, fields

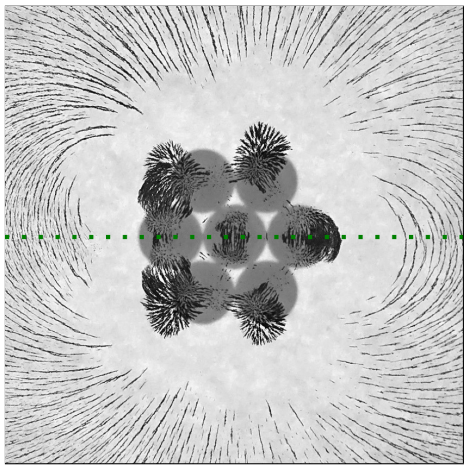

(d) $\alpha = 1$ misaligned state, filings

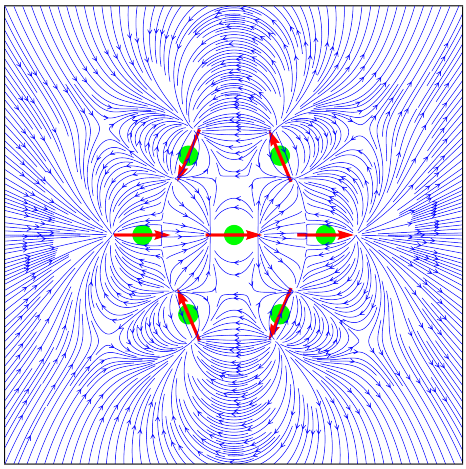

(e) $\alpha = 2.4$ dipolar state, fields

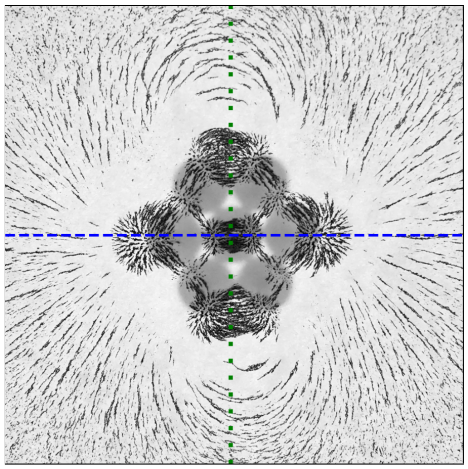

(f) $\alpha = 2.4$ dipolar state, filings

FIG. 2. Predictions (left panels) and observations (right panels) of the circular, misaligned, and dipolar states. In the left panels, green dots show the positions of the seven dipoles, red arrows show the directions of their dipole moments, and directed blue lines show magnetic field lines $\mathbf{B}(x, y, 0.5)$ given by Eq. (10). The right panels show the positions of seven 5 mm magnet spheres (grey discs), iron filings (black) on the surface of a piece of paper resting atop the seven magnets, reflection planes (green dotted lines), and time-reversed reflection planes (blue dashed lines).

both stable to small perturbations for $\alpha_1 < \alpha < \alpha_2$. If α comes into this intermediate range by increasing through α_1, the system will be in the circular state. Continuing to increase α through α_2 results in an abrupt phase transition to the dipolar state. If α comes into the intermediate range by decreasing through α_2, the system will be in the dipolar state. Continuing to decrease α through α_1 results in an abrupt phase transition to the circular state.

Thus, despite having only seven degrees of freedom, our seven-magnet system features nonlinear phase transitions and hysteresis reminiscent of the Ising model, which involves large quantities of dipoles.[24,25]

Contributions of this paper include: (a) identifications, symmetry classifications, and observations of the circular, misaligned, and dipolar states and (b) calculation of the range $\alpha_1 < \alpha < \alpha_2$ over which the circular and dipolar states are both stable.

In a companion paper, we explore the normal modes of oscillation about these states.[26]

II. SYSTEM DESCRIPTION

We consider the rotational motion of seven dipoles that are arranged to form a filled regular hexagon in the $x-y$ plane, with their dipole moments confined to this plane. The dipoles are free to rotate about fixed axes in the z direction (Fig. 1). Adjacent dipoles are separated by a distance a. Dimensionless positions of the six perimeter dipoles are measured in units of a, and are given by

$$\mathbf{p}_i = \left\{ \cos\left[2\pi\frac{(i-1)}{6}\right],\ \sin\left[2\pi\frac{(i-1)}{6}\right],\ 0 \right\}, \tag{1}$$

where $i = 1, 2, \cdots, 6$.

The magnitude of the dipole moment of each of the six perimeter dipoles is denoted by m. Dimensionless magnetic moments of these dipoles are measured in units of m and are given by (Fig. 1)

$$\mathbf{m}_i = (\cos\phi_i,\ \sin\phi_i,\ 0), \tag{2}$$

where ϕ_i is the angle between the magnetic moment of dipole i and the x axis, measured counterclockwise from the x axis in the $x-y$ plane.

The dimensionless position of the central dipole, measured in units of a, is given by

$$\mathbf{p}_0 = (0,0,0), \tag{3}$$

and its dimensionless magnetic dipole moment, measured in units of m, is given by (Fig. 1)

$$\mathbf{m}_0 = \alpha(\cos\phi_0, \sin\phi_0,\ 0). \tag{4}$$

Here,

$$\alpha = \frac{m_0}{m} \tag{5}$$

is the ratio of the magnitudes of the dipole moments of the central and perimeter dipoles. The angle ϕ_0 is the angle between the magnetic moment of the central dipole and the x axis, measured counterclockwise from the x axis in the $x-y$ plane.

The energy scale of interaction between two perimeter dipoles is given by

$$U_0 = \frac{\mu_0 m^2}{4\pi a^3}. \tag{6}$$

The dimensionless magnetostatic potential energy of the system is measured in units of U_0, and is given by the sum over all pairwise interactions,[27]

$$U = \sum_{i=0}^{5}\sum_{j=i+1}^{6} \frac{\mathbf{m}_i\cdot\mathbf{m}_j - 3(\mathbf{m}_i\cdot\hat{\mathbf{r}}_{ij})(\mathbf{m}_j\cdot\hat{\mathbf{r}}_{ij})}{r_{ij}^3}, \tag{7}$$

where $\mathbf{r}_{ij} = \mathbf{p}_j - \mathbf{p}_i$ is the dimensionless position of dipole j relative to dipole i, $r_{ij} = |\mathbf{r}_{ij}|$ is the magnitude of this vector, and $\hat{\mathbf{r}}_{ij} = \mathbf{r}_{ij}/r_{ij}$ is the unit vector that points in the direction of $\mathbf{r}_{ij}$. Using the foregoing, U can be expressed in terms of the seven orientation angles ϕ_i (for $i = 0, 1, \cdots, 6$), which are free to respond to the magnetic torques of the other six magnets.

To distinguish between different equilibrium states, we consider the dimensionless net dipole moment of the seven dipoles

$$\mathbf{M} = \sum_{i=0}^{6} \mathbf{m}_i. \tag{8}$$

The magnetic field scale is

$$B_0 = \frac{\mu_0 m}{4\pi a^3}. \tag{9}$$

The dimensionless magnetic field strength $\mathbf{B}$ at dimensionless position $\mathbf{r}$ is measured in units of B_0, and is given by[27]

$$\mathbf{B}(\mathbf{r}) = \sum_{i=0}^{6} \left[3\frac{\mathbf{m}_i \cdot (\mathbf{r}-\mathbf{p}_i)}{|\mathbf{r}-\mathbf{p}_i|^5}(\mathbf{r}-\mathbf{p}_i) - \frac{\mathbf{m}_i}{|\mathbf{r}-\mathbf{p}_i|^3} \right]. \tag{10}$$

The process of finding the stable equilibria of this system is equivalent to finding the local minima of U as a function of the seven orientation angles ϕ_i. This is performed numerically for $\alpha = 1$ using the minimization function "minimize" from the Sage computer math library using 5000 random initial states in order to identify all stable equilibrium states. We achieve each random initial state by assigning seven random numbers between 0 and 2π to the seven orientation angles ϕ_i.

In comparing theory with experiments, it is also useful to investigate unstable equilibrium states such as saddle points in the potential energy. For this purpose we calculate the sum of squares of the magnitudes of the torques on the seven dipoles,[18]

$$Q = \sum_{i=0}^{6} \left(\frac{\partial U}{\partial \phi_i} \right)^2. \tag{11}$$

Q is never negative and its zeroes correspond to equilibrium states, where the torques on all of the dipoles vanish. Thus, at both stable and unstable equilibrium points, Q reaches a minimum value of $Q = 0$. Q can also reach minima where $Q > 0$; such minima are not equilibrium states. We identified minima with $Q < 10^{-11}$ as equilibrium states.

Minimizing U yields stable equilibrium states and finding zeros of Q yields all of the equilibrium states. In practice, finding zeros of Q gives better convergence than minimizing U for barely stable equilibria by providing a larger basin of attraction for the minimization procedure. We used the Sage computer math library function "diff" to carry out the partial derivatives of Eq. (11) in closed form. Doing so reduces Q to a function of the seven orientation angles ϕ_i.

To test the stability of equilibrium states, we examine the seven eigenvalues of the Hessian of the potential energy,

$$(\mathbf{H}U)_{i,j} = \frac{\partial^2 U}{\partial \phi_i \delta \phi_j}. \tag{12}$$

The equilibrium is stable if all seven eigenvalues are positive. As α varies, equilibrium states pass through critical points where their stability changes. We detect these critical points by watching for sign changes in the determinant of the Hessian. This method works because the determinant of a matrix is equal to the product of its eigenvalues; when the number of positive eigenvalues changes, the sign of the determinant also changes (excluding the special case that an even number of eigenvalues change sign simultaneously). After ascertaining that a state is stable for a particular value of α by explicitly calculating the eigenvalues, we simply calculate the values of the determinant for other values of α to determine where the state ceases to be stable.

III. STATES FOR $\alpha = 1$

In this section, we investigate the equilibrium states for $\alpha = 1$, for which all seven dipoles have the same strength. Finding zeros of Q yields 504 equilibrium states. Eliminating redundant states by considering reflections and rotations leaves 54 distinct equilibrium states for $\alpha = 1$. Figure 3 shows the energies of these 54 states, 30 of which are 12-fold redundant (solid green lines) and 24 of which are 6-fold redundant (dotted red lines). The three lowest-energy states are, in order of increasing energy, the stable "circular" state, the unstable "misaligned" state, and the unstable "dipolar" state.

Figures 4(a)-(c) show the magnetic configurations of these three states for $\alpha = 1$. In the circular state (a), the perimeter dipole moments circle around the center dipole and the center dipole moment points toward the center of a perimeter dipole. In the misaligned state (b), the perimeter dipole moments again circle around the center dipole, but the center dipole moment points toward the point of contact between two perimeter dipoles. In the dipolar state (c), the perimeter dipole arrangement has the same symmetry as the magnetic field of the center dipole.

It is instructive to consider the symmetries of these three states. Doing so requires care because magnetic moments such as those shown in Fig. 4 are pseudovectors, or "axial vectors," which behave differently under reflections than true, or "polar,"

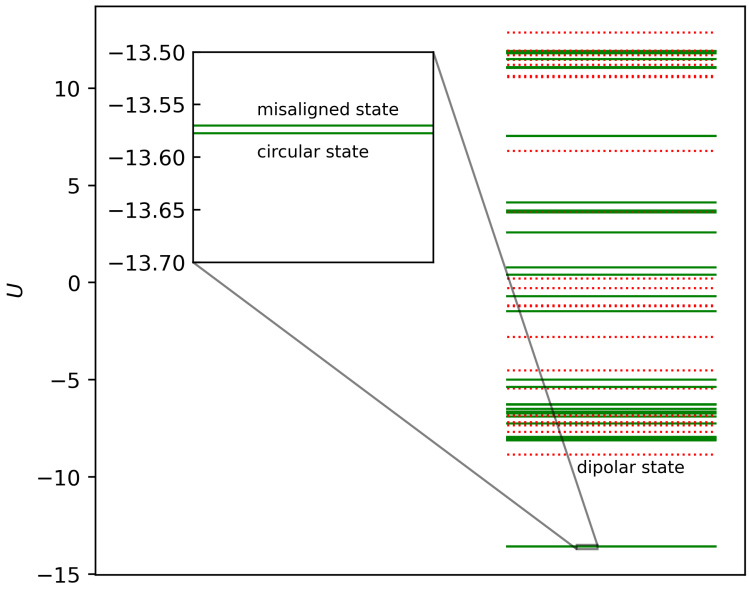

FIG. 3. Magnetostatic potential energies U of 54 distinct states for $\alpha = 1$. Of these states, 30 are 12-fold redundant (green solid lines) and 24 are 6-fold redundant (red dotted lines). The energy splitting of the two lowest-energy states is shown in the inset. At $\alpha = 1$, the circular state has the lowest energy and is stable, the misaligned state has the next-lowest energy (just slightly higher than the circular state) and is unstable, and the dipolar state has the third-lowest energy and is also unstable.

vectors such as the position vector.[28] The reflection of a polar vector is the same as its mirror image, meaning that its components parallel to the reflection plane remain the same and its component perpendicular to the reflection plane is reversed. In contrast, the reflection of an axial vector is opposite to its mirror image, meaning that its components parallel to the reflection plane are reversed and its component perpendicular to the reflection plane remains the same. Magnetic moments and magnetic fields are axial vectors because reflections of electric currents yield magnetic moments and magnetic fields that are opposite to their mirror images.[29]

Accordingly, the circular state of Fig. 4(a) is symmetric under reflection about the $x = 0$ plane (green dotted line). This reflection operation is denoted by m_x. The point-group symmetry of the circular state is $m(E, m_x)$, where E is the identity operation.[30] The misaligned state of Fig. 4(b) is symmetric under reflection m_y about the $y = 0$ plane (green dotted line) and has point-group symmetry $m(E, m_y)$.

The dipolar state of Fig. 4(c) is symmetric under three operations: reflection m_x about the $x = 0$ plane (green dotted line), time-reversed reflection m'_y about the $y = 0$ plane (blue dashed line), and time-reversed 180-degree (two-fold) rotation $2'_z$ about the z axis (perpendicular to the plane of the figure). A time-reversed reflection is a reflection followed by a time reversal, and a time-reversed rotation is a rotation followed by a time reversal. A time reversal, denoted by a prime on the operation, has no effect on the positions of the dipoles, but re-

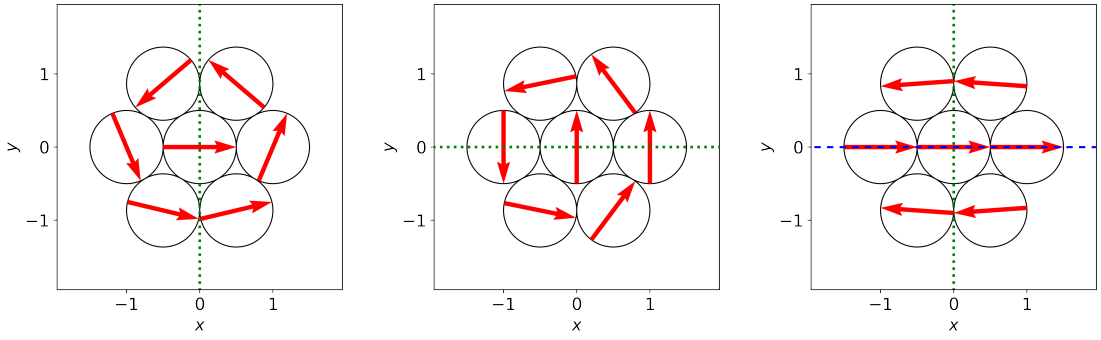

(a) $\alpha = 1$ circular state, stable

(b) $\alpha = 1$ misaligned state, unstable

(c) $\alpha = 1$ dipolar state, unstable

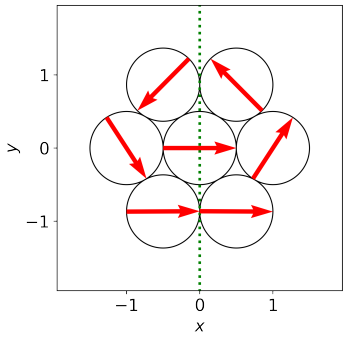

(d) $\alpha = 1.5$ circular state, stable

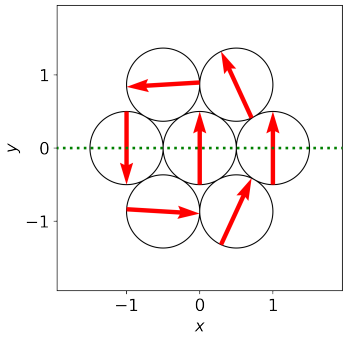

(e) $\alpha = 1.5$ misaligned state, unstable

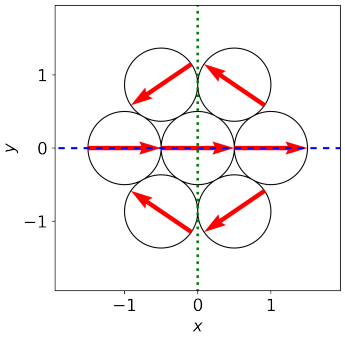

(f) $\alpha = 1.5$ dipolar state, metastable

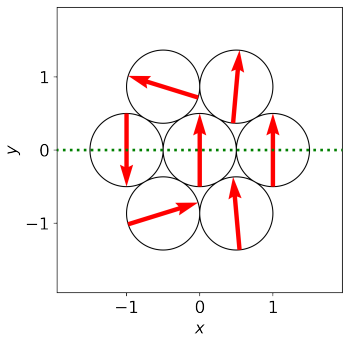

(g) $\alpha = 3$ misaligned state, unstable

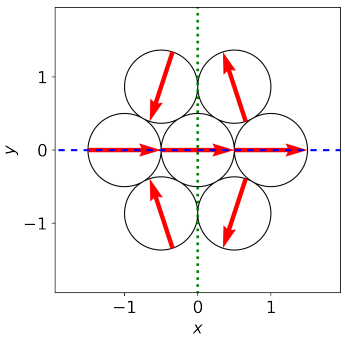

(h) $\alpha = 3$ dipolar state, stable

FIG. 4. Circular, misaligned, and dipolar states for relative central dipole strengths $\alpha = 1$, 1.5, and 3. Arrows indicate dipole moment directions, green dotted lines indicate reflection planes, and blue dashed lines indicate time-reversed reflection planes.

verses the directions of their magnetic moments by reversing the directions of the currents that produce these moments, as if time were running backwards. Thus, the point-group symmetry of the dipolar state of Fig. 4(c) is $mm'2'(E, m_x, m'_y, 2'_z)$.

We now explain the 12-fold and 6-fold redundancies of Fig. 3. Our minimization procedure places no constraints on the directions of the seven dipole moments, but does constrain the positions of the seven dipoles to coincide with those shown in Fig. 1. For $\alpha = 1$, this procedure finds six redundant circular states with perimeter dipole moments circling counterclockwise, including Fig. 4(a) and rotations of this figure by 60°, 120°, 180°, 240°, and 300°. This procedure also finds six redundant circular states with perimeter dipole moments circling clockwise; these six states can be obtained from the six counterclockwise states by applying a time-reversed reflection about the plane that contains the center dipole moment and is perpendicular to the plane of the hexagon. For Fig. 4(a), for example, this plane is the $y = 0$ plane and the associated time-reversed reflection m'_y produces a redundant state with the dipole moments circling clockwise. Thus, the $\alpha = 1$ circular state is 12-fold redundant. Similar logic shows that the misaligned state is also 12-fold redundant.

The dipolar state is only 6-fold redundant because the time-reversed reflection about the plane containing the center dipole moment is a symmetry operation for this state, and does not produce a new redundant state. For Fig. 4(c), for example, this plane is the $y = 0$ plane (blue dashed line) and the associated time-reversed reflection m'_y produces a state that is identical to Fig. 4(c).

IV. STATES FOR GENERAL α

In this section, we investigate the stability of the circular, misaligned, and dipolar states for general α. Shown in Fig. 5 are the respective determinants $|\mathbf{H}U_\mathrm{c}|$, $|\mathbf{H}U_\mathrm{m}|$, and $|\mathbf{H}U_\mathrm{d}|$ of the Hessian for these states as a function of α. The sign of the determinant indicates stability to small perturbations, with a positive determinant indicating stability (solid traces) and a negative determinant indicating instability (dashed traces).

The *circular state* is stable for $0 < \alpha < \alpha_2$ and does not exist for $\alpha > \alpha_2$, where $|\mathbf{H}U_\mathrm{c}|$ and the orientation angles ϕ_i are complex (Fig. 5). For α approaching α_2 from below, the behaviors of $|\mathbf{H}U_\mathrm{c}|$ and ϕ_i are strongly nonlinear, with the derivative of $|\mathbf{H}U_\mathrm{c}|$ approaching $-\infty$. A least squares fit to the form

$$|\mathbf{H}U| = A(\alpha_2 - \alpha)^n \tag{13}$$

gives $A = 14932$, $\alpha_2 = 2.4724$, and $n = 0.5040$. The nearness of n to $1/2$ suggests that the square of the determinant is approximately linear for $\alpha \lesssim \alpha_2$. Accordingly, a least-squares fit to the linear form

$$|\mathbf{H}U|^2 = C(\alpha_2 - \alpha) \tag{14}$$

gives $C = 2.094007 \times 10^8$ and $\alpha_2 = 2.472448$. Both fits agree on the value

$$\alpha_2 = 2.4724 \tag{15}$$

to within five significant figures.

The *misaligned state* is unstable for all $\alpha > 0$ (Fig. 5). For small α, $|\mathbf{H}U_\mathrm{m}| \approx -|\mathbf{H}U_\mathrm{c}|$.

The *dipolar state* is stable for $\alpha > \alpha_1$ and unstable for $0 < \alpha < \alpha_1$ (Fig. 5). To find α_1, we set $\phi_0 = 0$, exploit Eq. (2) to define Cartesian components of the dimensionless perimeter dipole moments (for $i = 1, 2, \ldots, 6$),

$$x_i = \cos\phi_i \tag{16a}$$
$$y_i = \sin\phi_i \tag{16b}$$

and invoke the symmetry relationships

$$x_2 = x_3 = x_5 = x_6 \tag{17a}$$
$$y_2 = y_5 = -y_3 = -y_6 \tag{17b}$$

to convert the system of equilibrium trigonometric equations into a system of multivariate quadratic polynomial equations. We rearrange these equations into a single quartic polynomial and use the quartic formula to obtain exact general expressions for the ϕ_i and $|\mathbf{H}U_\mathrm{d}|$ as a function of α. Finding the zero of $|\mathbf{H}U_\mathrm{d}|$ gives

$$\alpha_1 = 1.154460452378. \tag{18}$$

Curiously, $|\mathbf{H}U_\mathrm{d}| = 0$ at $\alpha = 2.05$ (Fig. 5). Because $|\mathbf{H}U_\mathrm{d}| > 0$ on either side of this zero, the

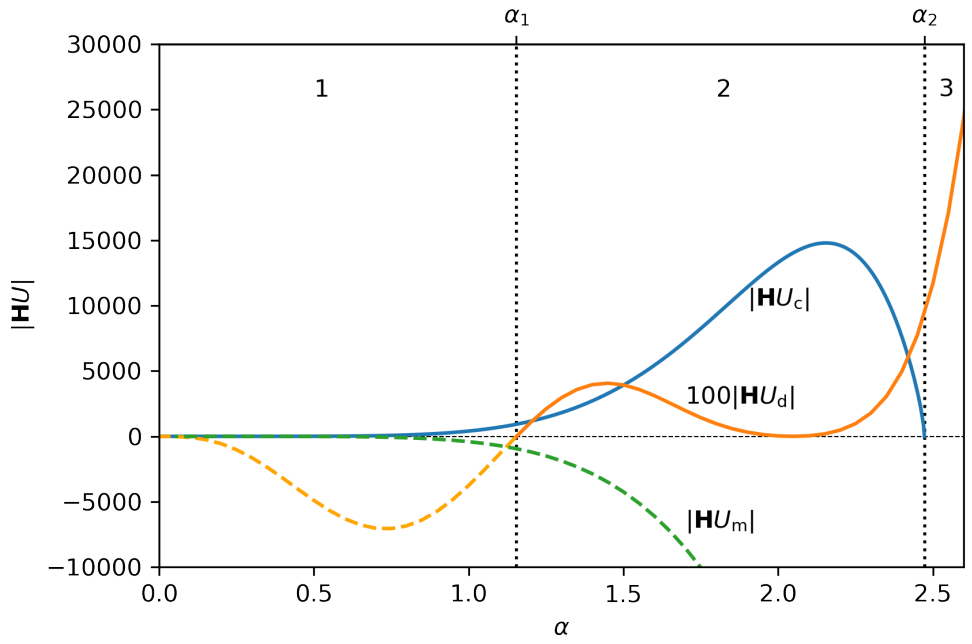

FIG. 5. Determinants $|\mathbf{H}U_\mathrm{c}|$, $|\mathbf{H}U_\mathrm{m}|$, and $|\mathbf{H}U_\mathrm{d}|$ of the Hessian for the respective circular, misaligned, and dipolar states as a function of the relative strength α of the center dipole. The dipolar determinant is multiplied by 100 to improve visibility. Positive determinants imply stability to small perturbations and are denoted by solid traces. Negative determinants imply instability and are denoted by dashed traces. The circular state is stable for $\alpha < \alpha_2 = 2.47$, above which the state ceases to exist. The dipolar state is stable for $\alpha > \alpha_1 = 1.15$ and unstable for $\alpha < \alpha_1$. The misaligned state is unstable for all α. Numerals indicate stability regions 1, 2, and 3 (Table I).

zero corresponds to a point of neutral stability surrounded by a region of stability. As discussed in a companion paper, one of the modes of oscillation vanishes at this point.[26]

The foregoing identifies three stability regions that are summarized in Table I and are indicated in Fig. 5. In region 1, only the circular state is stable. In region 2, both the circular and the dipolar states are stable. And in region 3, only the dipolar state is stable.

TABLE I. Stability regions.

Region	Range	Stable State(s)	Illustration(s)
1.	$\alpha < \alpha_1$	circular	Fig. 4(a)
2.	$\alpha_1 < \alpha < \alpha_2$	circular, dipolar	Figs. 4(d), (f)
3.	$\alpha > \alpha_2$	dipolar	Fig. 4(h)

Figure 4 shows magnetic configurations of the circular, misaligned, and dipolar states for $\alpha = 1$, $\alpha = 1.5$, and $\alpha = 3$, which respectively illustrate regions 1, 2, and 3. The circular state does not exist in region 3, which explains the missing panel in the lower left corner of Fig. 4. The point group symmetries for the circular, misaligned, and dipolar states at $\alpha = 1$ (Sec. III) evidently apply to other values of α as well. The magnetic field of each state has the same symmetries as its dipoles.

Figure 6 shows the energies of the circular, misaligned, and dipolar states as a function of α, with stable states denoted by solid traces and unstable states denoted by dashed traces. In region 1, the perimeter dipoles dominate the magnetic interactions and only the circular state is stable. In region 2, the circular and dipolar states are both stable to small perturbations. Within this region, the circular

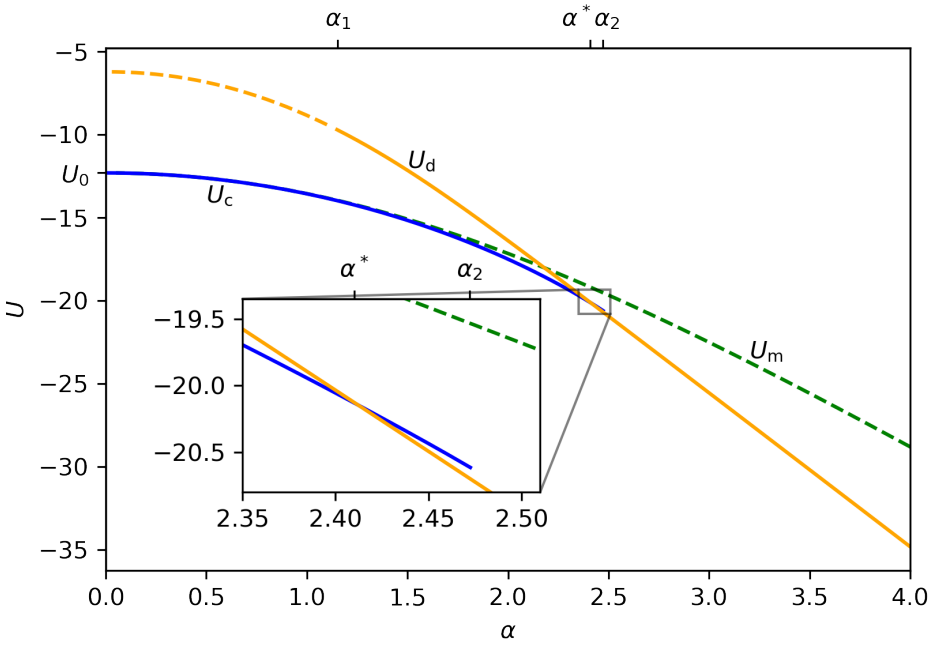

FIG. 6. Magnetostatic potential energies U_c, U_m, and U_d of the circular, misaligned, and dipolar states vs. the relative strength α of the central dipole. Solid traces denote states that are stable to small perturbations and dashed traces denote unstable states. Indicated are the critical values $\alpha_1 = 1.15$ and $\alpha_2 = 2.47$ between which the circular and dipolar states are both stable, and the value $\alpha^* = 2.41$ at which their energies match. The inset shows detail near α^* and α_2.

state has the lower energy for $\alpha < \alpha^* = 2.41$, where the dipolar state is metastable, and the dipolar state has the lower energy for $\alpha > \alpha^*$, where the circular state is metastable. A "metastable" state is stable to small perturbations but unstable to large ones because its energy is not a global minimum. In region 3, the center dipole dominates the magnetic interactions, the dipolar state is stable, and the circular state does not exist.

The system exhibits hysteresis (Fig. 6). The circular state is stable at $\alpha = 0$ and remains stable for increasing α until $\alpha > \alpha_2$ (region 3), where the circular state vanishes and the system converts spontaneously to the dipolar state. For decreasing α, the dipolar state remains stable until $\alpha < \alpha_1$ (region 1), where it becomes unstable and the system reverts to the circular state. The circular and dipolar states are both stable to small perturbations over the intermediate range $\alpha_1 < \alpha < \alpha_2$ (region 2), where the state of the system is determined by its history.

As $\alpha \to 0$, the influence of the central dipole vanishes and the energies of the circular and misaligned states converge to[22] (Fig. 6)

$$U_0 = -\frac{5\sqrt{3}}{6} - \frac{87}{8} = -12.318. \qquad (19)$$

At $\alpha = 0$ for both of these states, the moments of the six perimeter dipoles point tangent to a circle of unit radius and the configuration has six-fold rotational symmetry 6_z about the z axis. Thus, the perimeter dipoles in the circular and misaligned states are perfectly circular for $\alpha = 0$.

The circular and misaligned states depart from perfect circularity for $\alpha > 0$, with these departures becoming more and more pronounced as α increases (Fig. 4).

For the dipolar state as $\alpha \to \infty$, the central dipole dominates and the perimeter dipoles align exactly

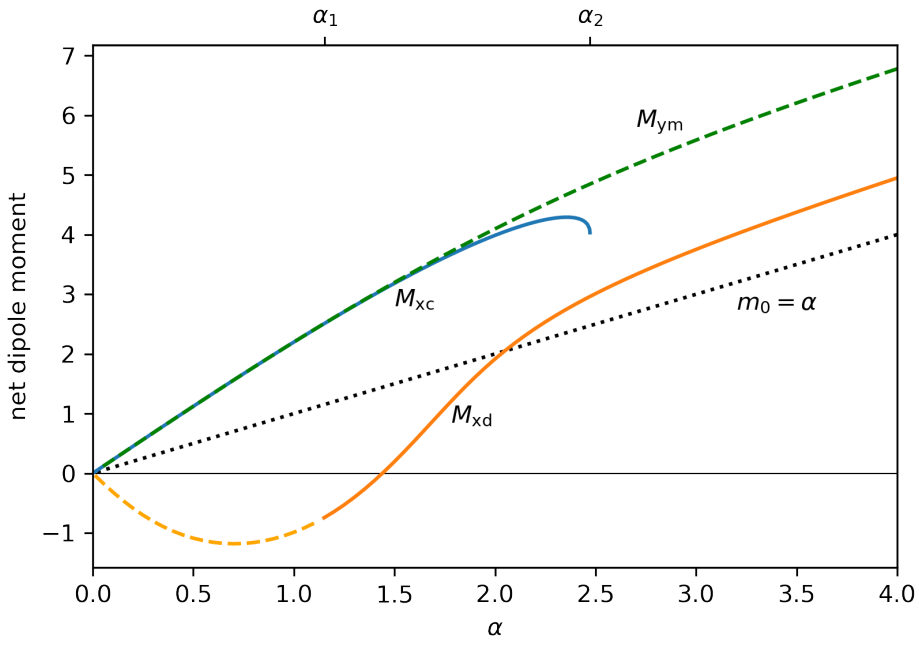

FIG. 7. Components M_{xc}, M_{ym}, and M_{xd} of the net dipole moment for the respective circular, misaligned, and dipolar states from Eq. (22) vs. α. Solid traces denote locally stable states and dashed traces denote unstable states. Indicated also are the critical values $\alpha_1 = 1.15$ and $\alpha_2 = 2.47$ between which the circular and dipolar states are both locally stable. The magnitude of the central dipole moment, $m_0 = \alpha$, is also shown as a dotted line. At the intersection $M_{xd} = m_0$, the net dipole moment of the perimeter magnets of the dipolar state vanishes. This intersection occurs at $\alpha = 2.05$, where $|\mathbf{H}U_d| = 0$ (Fig. 5).

with the magnetic field of the central dipole. The $i = 0$ term of Eq. (10) describes the field of this dipole, which overwhelms the other six terms as $\alpha \to \infty$. In this limit, the magnetic field at the location $\mathbf{r} = \mathbf{p}_2 = (1/2,\ \sqrt{3}/2,\ 0)$ of dipole $\mathbf{m}_2$ is given by

$$\mathbf{B}(\mathbf{p}_2) = \frac{\alpha}{4}\left(-1,\ 3\sqrt{3},\ 0\right), \tag{20}$$

obtained by inserting Eqs. (1), (3), and (4) with $\phi_0 = 0$ into Eq. (10). Aligning dipole $\mathbf{m}_2$ with this field gives the orientation angle ϕ_2 of this dipole in the $\alpha \to \infty$ limit,

$$\phi_\infty = \pi - \tan^{-1}\left(3\sqrt{3}\right) \approx 100.9^\circ. \tag{21}$$

The other orientation angles follow by symmetry. As α decreases, the influence of the central dipole diminishes and the directions of the perimeter dipole moments depart increasingly from the field of the central dipole (Fig. 4), while retaining the symmetry of the dipolar state.

The reflection symmetry of a state determines the direction of its net dipole moment $\mathbf{M}$, which must be unchanged under reflection. Being the sum of axial vectors according to Eq. (8), $\mathbf{M}$ must also be an axial vector. As discussed above, the components of an axial vector that are parallel to a reflection plane are reversed under reflection. But $\mathbf{M}$ must be unchanged under reflection. Consequently, $\mathbf{M}$ must have no components that are parallel to the reflection plane; it must therefore point normal to the reflection plane. Accordingly, owing to the m_x, m_y, and m_x reflection symmetries of the circular, misaligned, and dipolar states shown in Figs. 4(a), (b),

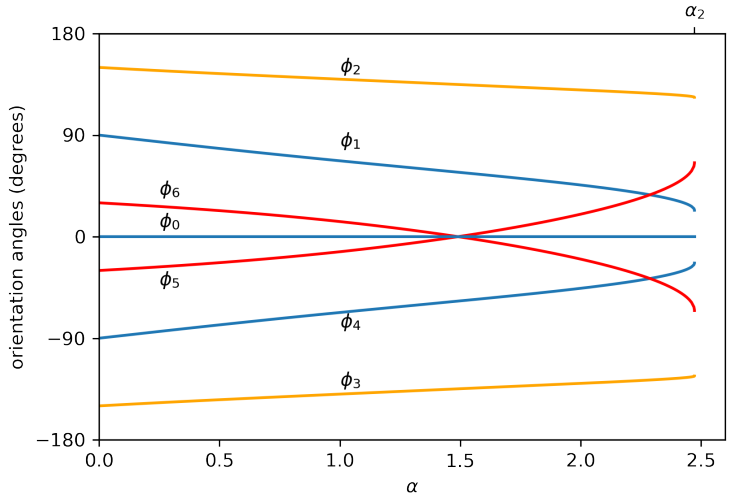

(a) circular state

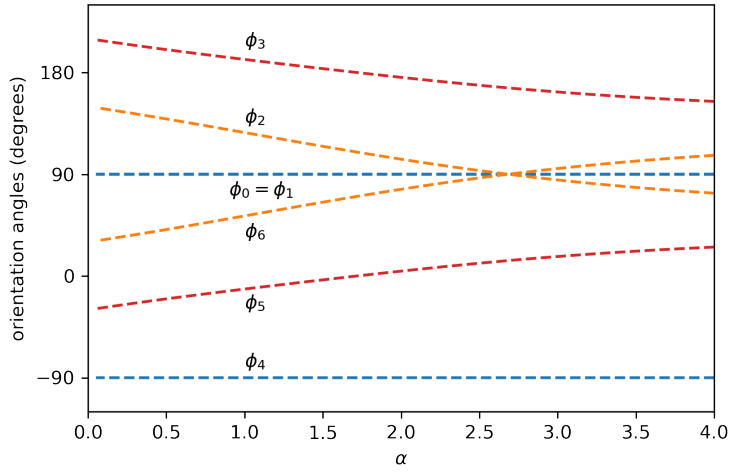

(b) misaligned state

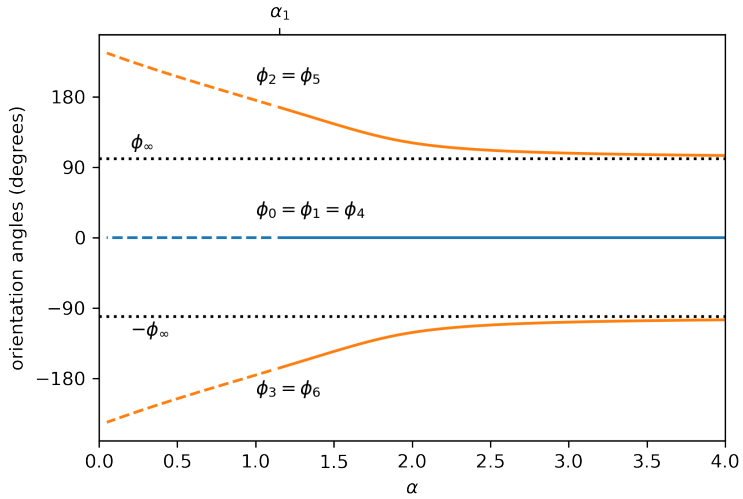

(c) dipolar state

FIG. 8. Predicted equilibrium orientation angles vs. α for the circular (a), misaligned (b), and dipolar (c) states (Fig. 4). The circular state is stable (solid traces) for $\alpha < \alpha_2 = 2.47$ and does not exist for $\alpha > \alpha_2$. The misaligned state is unstable (dashed traces) for all α. The dipolar state is unstable (dashed traces) for $\alpha < \alpha_1 = 1.15$ and stable (solid traces) for $\alpha > \alpha_1$. For the dipolar state, dotted lines give the $\alpha \to \infty$ asymptotes $\phi \to \pm\phi_\infty = \pm 100.9^\circ$ from Eq. (21).

and (c), respectively, the net dipole moments for these states take the forms

$$\mathbf{M}_{\rm c} = M_{x\rm c}\hat{\mathbf{x}} \tag{22a}$$

$$\mathbf{M}_{\rm m} = M_{y\rm m}\hat{\mathbf{y}} \tag{22b}$$

$$\mathbf{M}_{\rm d} = M_{x\rm d}\hat{\mathbf{x}}. \tag{22c}$$

The α dependencies of the components $M_{x\rm c}$, $M_{y\rm m}$, and $M_{x\rm d}$ of these vectors are shown in Fig. 7. Because $M_{x\rm c} > 0$ and $M_{y\rm m} > 0$ for $\alpha > 0$, the net dipole moments of the circular and misaligned states point in the same direction as the central dipole for all $\alpha > 0$ [in the $+x$ and $+y$ directions, respectively; Figs. 4(a), (b), (d), (e), and (g)]. But because $M_{x\rm d} < 0$ for $\alpha < 1.45$, the net dipole moment of the dipolar state points opposite to the central dipole (in the $-x$ direction) for $\alpha < 1.45$ [Fig. 4(c)], and points in the same direction as the central dipole (in the $+x$ direction) for $\alpha > 1.45$ [Fig. 4(f), (h)].

Also shown in Fig. 7 is the magnitude of the central dipole moment, $m_0 = \alpha$. At the intersection $M_{x\rm d} = m_0$, the net dipole moment of the perimeter magnets of the dipolar state vanishes. This intersection occurs at $\alpha = 2.05$, where $|\mathbf{H}U_{\rm d}| = 0$ (Fig. 5).

Figures 8(a)-(c) show predicted equilibrium orientation angles vs. α for the circular, misaligned, and dipolar states, respectively. These figures show that the $\alpha = 1$ symmetries discussed in Sec. III persist for $\alpha \neq 1$. Figure 8(a) shows nonlinear changes in the orientation angles near α_2, where the circular state disappears.

V. EXPERIMENTAL OBSERVATIONS

To observe the circular, misaligned, and dipolar states, we use standard commercially available nickel-coated "strong" magnet spheres of diameter 5 mm and partially magnetized "weak" magnets of the same size that we obtained from the same manufacturer.[23] Using a magnet in the center of the hexagon whose strength differs from the strength of the perimeter magnets allows us to explore equilibrium states for values of α that differ from unity.

Using a Hall-effect magnetometer, we measure the magnitude $B_{\rm w}$ of the magnetic field at the poles of about 100 weak magnets. For our experiments, we select six of these with field magnitudes satisfying

$$B_{\rm w} = 0.20 \pm 0.01 \text{ T}. \tag{23}$$

We also measure the magnitude $B_{\rm s}$ of the magnetic field at the poles of about 20 strong magnets. For our experiments, we select seven of these with field magnitudes satisfying

$$B_{\rm s} = 0.48 \pm 0.01 \text{ T}. \tag{24}$$

The magnitude of the magnetic field at the pole of a magnetic dipole is proportional to the magnitude of its dipole moment [Eq. (10)]. Accordingly, Eq. (5) gives

$$\alpha = 0 \tag{25}$$

for six strong magnets in the perimeter and no magnet at the center,

$$\alpha = \frac{B_{\rm w}}{B_{\rm s}} = 0.42 \pm 0.02 \tag{26}$$

for a weak magnet at the center and six strong magnets in the perimeter,

$$\alpha = \frac{B_{\rm s}}{B_{\rm s}} = 1.00 \pm 0.03 \tag{27}$$

for a strong magnet at the center and six strong magnets in the perimeter, and

$$\alpha = \frac{B_{\rm s}}{B_{\rm w}} = 2.4 \pm 0.1 \tag{28}$$

for a strong magnet at the center and six weak magnets in the perimeter.

We use iron filings to visualize magnetic fields produced by equilibrium configurations of magnet spheres, using the apparatus shown in Fig. 9. These filings reside on a piece of paper that is placed on top of the magnets. The piece of paper is tapped to align the filings with the fields. We use Eq. (10) to predict the fields $\mathbf{B}(x, y, 0.5)$ at the height $z = 0.5$ of the paper as a function of the horizontal coordinates x and y. In Figs. 10, 11, and 12, we compare the predicted field lines (left panels) and contours of constant B (right panels) with the patterns and symmetries of the iron filings (right panels), and find good general agreement.

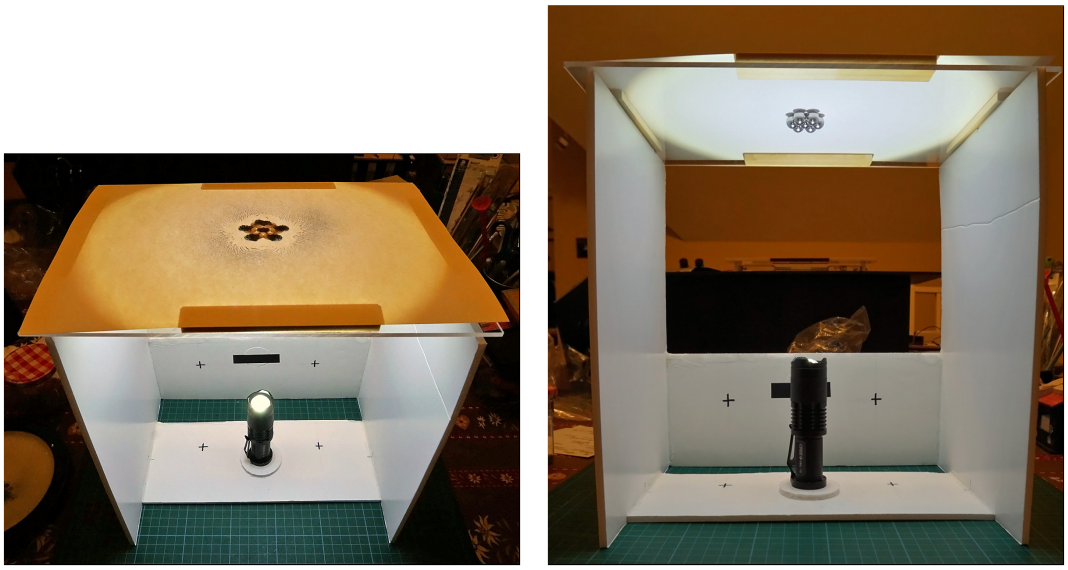

(a) view from above (b) view from below

FIG. 9. Experimental apparatus. A configuration of spherical neodymium magnets of diameter 5 mm is placed on a transparent sheet of plastic and a piece of paper is placed on the magnets. Iron filings are sprinkled on the paper and the paper is gently tapped. A flashlight is used from below to project a silhouette of the magnet positions onto the paper so that their locations can be known in relation to the iron-filing pattern. Photographs taken from above the paper show this silhouette and the pattern of iron filings (Figs. 2, 10, 11, and 12).

In Figs. 10, 11, and 12, clumps of filings gather where the fields are strong, robbing nearby weak-field regions of filings. For example, in Fig. 10(f), seven minima in the field strength are indicated by seven circular regions formed by weak-field $B = 2.0$ contours (solid violet traces). These regions are devoid of iron filings. Conversely, the strong-field $B = 4.5$ contours (dashed turquoise traces) tend to enclose regions with densely packed iron filings.

Far from the magnets in Figs. 10, 11, and 12, the forces on the iron filings are too weak to pull them into clumps but the torques are still strong enough to align them with the field (because $F \propto r^{-4}$ but $\tau \propto r^{-3}$). Arcs of iron filings thus show the direction of the magnetic fields projected onto the $z = 0.5$ plane, and agree with the predicted field lines.

Figure 10 shows the circular state for $\alpha = 0$, 0.42, 1, and 2.4, consistent with the predicted stability of this state for $\alpha < \alpha_2 = 2.47$ (Sec. IV). In addition to the $m(E, m_x)$ point group symmetry (Sec. III) that applies generally to the circular state, the $\alpha = 0$ circular state is symmetric under a six-fold rotation 6_z about the z axis, with the magnetic moments pointing tangent to a circle of unit radius [Fig. 10(a),(b)]. As the influence of the central magnet increases with increasing α, departures from this six-fold symmetry become more pronounced.

The misaligned state is predicted to be unstable for all α (Sec. IV), yet we observe it for $\alpha = 1$ at about the same frequency as the circular state (Fig. 11). As discussed in Sec. I, the misaligned state is easy to distinguish from the circular state experimentally because of differences between their planes of reflection symmetry relative to the perimeter magnets.

The dipolar state is predicted to be stable for $\alpha > \alpha_1 = 1.15$ (Sec. IV). Indeed, of our experimental values $\alpha = 0$, 0.42, 1, and 2.4, we observe the dipolar state only for $\alpha = 2.4$ (Fig. 12). This observation evidently obeys the point-group symmetry of this state, $mm'2'(E, m_x, m'_y, 2'_z)$.

Why is the misaligned state observed experimen-

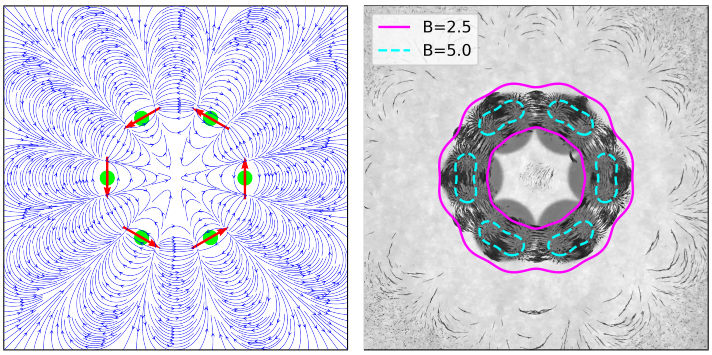

(a) $\alpha = 0$ circular state, fields

(b) $\alpha = 0$ circular state, filings

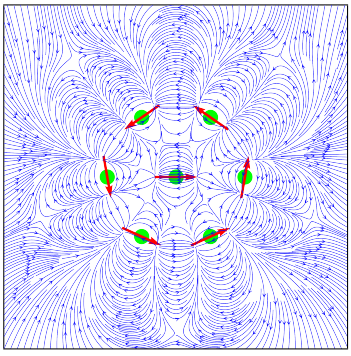

(c) $\alpha = 0.42$ circular state, fields

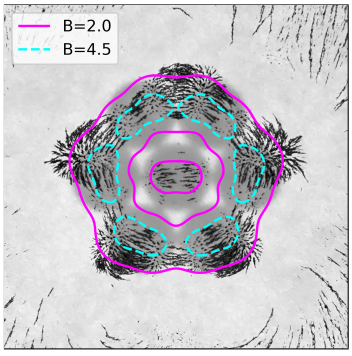

(d) $\alpha = 0.42$ circular state, filings

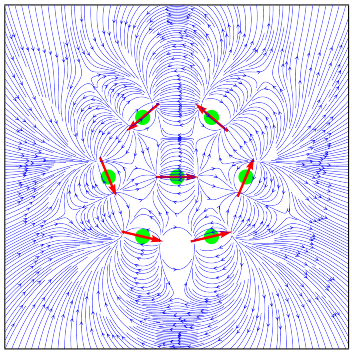

(e) $\alpha = 1$ circular state, fields

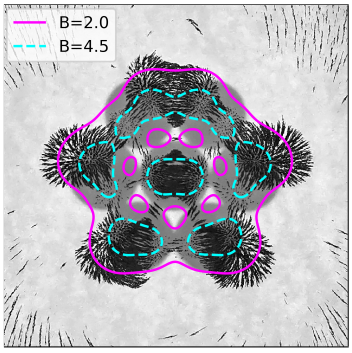

(f) $\alpha = 1$ circular state, filings

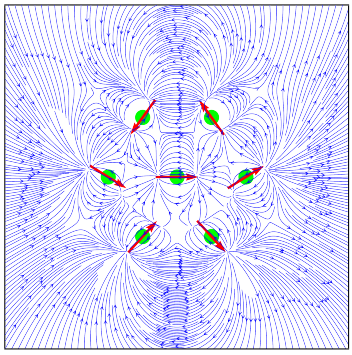

(g) $\alpha = 2.4$ circular state, fields

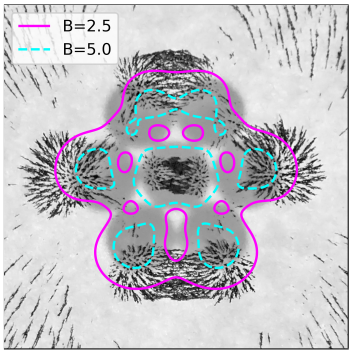

(h) $\alpha = 2.4$ circular state, filings

FIG. 10. Predictions (left panels) and observations (right panels) of the circular state for various values of α, similar to Fig. 2. The right panels show contours of constant $B(x, y, 0.5)$ obtained from Eq. (10).

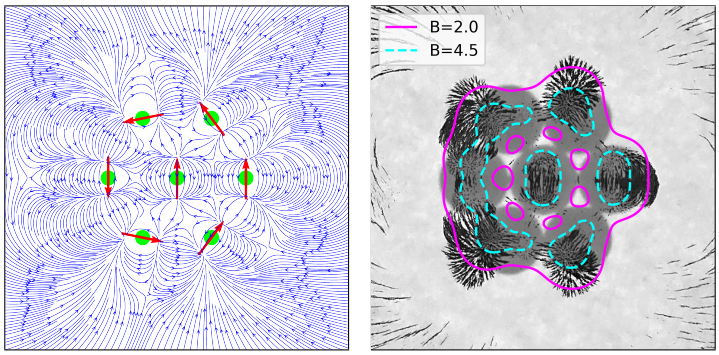

(a) $\alpha = 1.0$ misaligned state, fields (b) $\alpha = 1.0$ misaligned state, filings

FIG. 11. Prediction (a) and observation (b) of the misaligned state for $\alpha = 1$, similar to Fig. 10.

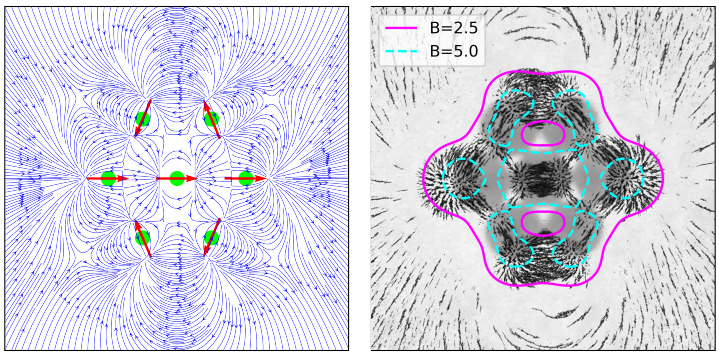

(a) $\alpha = 2.4$ dipolar state, fields (b) $\alpha = 2.4$ dipolar state, filings

FIG. 12. Prediction (a) and observation (b) of the dipolar state for $\alpha = 2.4$, similar to Fig. 10.

tally when it is predicted to be unstable? One possibility is that friction between magnet spheres, which is not included in our calculations, is sufficient to stabilize this state. But if friction is sufficient to stabilize the misaligned state for $\alpha = 1$, then why doesn't it stabilize the dipolar state at $\alpha = 1$?

The answer might lie in the relative degrees of instability of the misaligned and dipolar states. A negative eigenvalue of the Hessian of the potential energy renders a state unstable [Eq. (12)]. The $\alpha = 1$ misaligned state has one negative eigenvalue that is close to zero, -0.0833, meaning that the associated eigenmode is barely unstable. The $\alpha = 1$ dipolar state also has one negative eigenvalue, -0.373, but this eigenvalue is considerably more negative, meaning that the associated eigenmode is less stable than the unstable eigenmode of the misaligned state. This difference might enable friction to stabilize the barely unstable misaligned state but not the dipolar state.

Similarities between the misaligned and circular states offer further clues about the stability of the misaligned state. Despite the differences between their planes of reflection symmetry relative to the perimeter dipoles (Sec. III), the two states have similar potential energies, net dipole moments, reflection symmetries, and approximate pentagonal symmetries [Table II, Fig. 2(b), (d)]. As seen in Figs. 6 and 7, the potential energies and net dipole moments of the circular and misaligned states approach each other as $\alpha \to 0$ and are equal at $\alpha = 0$. And even at $\alpha = 1$, their differences are tiny (Fig. 3, Table II). These tiny differences may help to explain how friction can stabilize what would otherwise be an

unstable state.

The potential energy and net dipole moment differences between the circular and dipolar states are much more pronounced (Table II). This might help to explain why frictional effects are insufficient to stabilize the dipolar state at $\alpha = 1$.

VI. CONCLUSION

We have predicted the magnetic configurations, symmetries, and stabilities of three equilibrium states of a filled hexagon arrangement of magnetic dipoles as a function of the ratio α of the inner dipole strength to the perimeter dipole strength. Using small neodymium magnet spheres, we observe the circular and dipolar states at values of α that are consistent with the predicted stability ranges of these states. We also observe the $\alpha = 1$ misaligned state, which is barely unstable theoretically. Patterns of iron filings for these states agree with their predicted magnetic fields.

We predict a hysteretic transition for variable α that might be accessible experimentally. For $\alpha < \alpha_1$, only the circular state is stable. For $\alpha_1 < \alpha < \alpha_2$, the circular and dipolar states are both locally stable. And for $\alpha > \alpha_2$, only the dipolar state is stable. The hysteresis loop can be realized by starting with $\alpha < \alpha_1$ in the circular state and by increasing α. We predict that the circular state will persist until $\alpha > \alpha_2$, where it is abruptly replaced by the dipolar state. Then for decreasing α, the dipolar state will persist until $\alpha < \alpha_1$, where it is abruptly replaced by the circular state.

Our observations supply preliminary experimental evidence of hysteresis. We observe the circular state for $\alpha = 0$, 0.42, 1, and 2.4, consistent with the predicted stability range $\alpha < \alpha_2 = 2.47$ of this state (Fig. 10). We also observe the dipolar state for $\alpha = 2.4$, consistent with the predicted stability range $\alpha > \alpha_1 = 1.15$ of this state (Fig. 12). Figures 10(h) and 12(b) show our observations of these states at $\alpha = 2.4$, with distinct differences in the symmetries of the iron filings that are consistent with the predicted symmetries of these states. These observations supply evidence that both states are stable over an intermediate region ($\alpha_1 < \alpha < \alpha_2$), a necessary condition for hysteresis.

Stronger experimental evidence of hysteresis might be obtained using an electromagnet at the center of the hexagon and permanent magnets in the perimeter, with the current through the electromagnet controlling the value of α. To minimize friction during this process, it would be useful to eliminate contact between the seven magnets by placing them on seven low-friction vertical spindles that pass through their centers. It would be interesting to see if doing so would preclude the misaligned state.

We investigate equilibrium states for which the positions and dipole moments of all seven magnets are coplanar. It would be interesting to investigate the consequences of relaxing these assumptions. We have performed preliminary calculations that allow one or more of the seven dipole moments to point out of the plane, while restricting the positions of the seven dipoles to the plane. None of the resulting equilibrium states is stable. This suggests the possibility that the stable equilibrium states of any planar configuration of magnetic dipoles have dipole moments that are also restricted to the plane.

TABLE II. Magnetostatic potential energies U and net dipole moments M_{xc}, M_{ym}, and M_{xd} of the $\alpha = 1$ circular, misaligned, and dipolar states, respectively, from Eqs. (7), (8), and (22). See Figs. 3, 6 and 7.

State	Potential Energy	Net Dipole Moment
circular	-13.577	2.1986
misaligned	-13.570	2.1989
dipolar	-8.853	-0.9901

VII. ACKNOWLEDGEMENTS

We gratefully acknowledge support from NSF Grant No. 1808225, fruitful discussions with Harold Stokes and Mark Riffe about symmetries, and D.P.E. Smith for assistance with the experimental observations.

[1] S. Qu, "The Zen Gallery." http://zenmagnets.com/gallery/ (accessed 20-May-2019), 2014.

[2] B. F. Edwards, "Educational Value of Neodymium Magnet Spheres: Expert Report in the matter of Zen Magnets, LLC, CPSC Docket No. 12-2, 10/20/2014 (Redacted)." https://drive.google.com/file/d/

0Bw7DdocNZGQgWThTb3VvUHYza2s/view (accessed 20-May-2019), 2014.

[3]B. F. Edwards, D. M. Riffe, J. . Ji, and W. A. Booth, "Interactions between uniformly magnetized spheres," *American Journal of Physics*, vol. 85, no. 2, pp. 130–134, 2017.

[4]B. F. Edwards and J. M. Edwards, "Dynamical interactions between two uniformly magnetized spheres," *European Journal of Physics*, vol. 38, no. 1, p. 015205, 2016.

[5]J.-Y. Ji, B. F. Edwards, J. A. Spencer, and E. D. Held, "Potential, field, and interactions of multipole spheres: Coated spherical magnets," *Journal of Magnetism and Magnetic Materials*, vol. 529, p. 167861, 2021.

[6]J. Weis and D. Levesque, "Chain formation in low density dipolar hard spheres: a Monte Carlo study," *Physical Review Letters*, vol. 71, no. 17, p. 2729, 1993.

[7]A. Clarke and G. Patey, "Ground state configurations of model molecular clusters," *The Journal of Chemical Physics*, vol. 100, no. 3, pp. 2213–2219, 1994.

[8]R. Messina, L. A. Khalil, and I. Stanković, "Self-assembly of magnetic balls: From chains to tubes," *Physical Review E*, vol. 89, no. 1, p. 011202, 2014.

[9]C. L. Hall, D. Vella, and A. Goriely, "The mechanics of a chain or ring of spherical magnets," *SIAM Journal on Applied Mathematics*, vol. 73, no. 6, pp. 2029–2054, 2013.

[10]D. Vella, E. du Pontavice, C. L. Hall, and A. Goriely, "The magneto-elastica: from self-buckling to self-assembly," *Proceedings of the Royal Society A: Mathematical, Physical and Engineering Sciences*, vol. 470, no. 2162, p. 20130609, 2014.

[11]D. S. Borges, H. J. Herrmann, H. A. Carmona, J. S. Andrade, and A. D. Araújo, "Patterns formed by chains of magnetic beads," in *EPJ Web of Conferences*, vol. 249, p. 15004, EDP Sciences, 2021.

[12]N. Vandewalle and S. Dorbolo, "Magnetic ghosts and monopoles," *New Journal of Physics*, vol. 16, no. 1, p. 013050, 2014.

[13]J. Boisson, C. Rouby, J. Lee, and O. Doaré, "Dynamics of a chain of permanent magnets," *EPL (Europhysics Letters)*, vol. 109, no. 3, p. 34002, 2015.

[14]J. Schönke and E. Fried, "Stability of vertical magnetic chains," *Proceedings of the Royal Society A: Mathematical, Physical and Engineering Sciences*, vol. 473, no. 2198, p. 20160703, 2017.

[15]N. Vandewalle and A. Wafflard, "Ground state of magnetocrystals," *Physical Review E*, vol. 103, no. 3, p. 032117, 2021.

[16]T. M. Hoang and D. V. Cortes, "Stability of magnetic rings," *International Journal of Solids and Structures*, vol. 225, p. 111060, 2021.

[17]G. L. Pollack and D. R. Stump, "Two magnets oscillating in each other's fields," *Canadian journal of physics*, vol. 75, no. 5, pp. 313–324, 1997.

[18]B. F. Edwards and J. M. Edwards, "Periodic nonlinear sliding modes for two uniformly magnetized spheres," *Chaos*, vol. 27, no. 5, 2017.

[19]B. F. Edwards, B. A. Johnson, and J. M. Edwards, "Periodic bouncing modes for two uniformly magnetized spheres. i. trajectories," *Chaos: An Interdisciplinary Journal of Nonlinear Science*, vol. 30, no. 1, p. 013146, 2020.

[20]B. F. Edwards, B. A. Johnson, and J. M. Edwards, "Periodic bouncing modes for two uniformly magnetized spheres. ii. scaling," *Chaos: An Interdisciplinary Journal of Nonlinear Science*, vol. 30, no. 1, p. 013131, 2020.

[21]P. T. Haugen and B. F. Edwards, "Dynamics of two freely rotating dipoles," *American Journal of Physics*, vol. 88, no. 5, pp. 365–370, 2020.

[22]D. R. Stump, G. L. Pollack, and J. Borysowicz, "Magnets at the corners of polygons," *American Journal of Physics*, vol. 65, no. 9, pp. 892–897, 1997.

[23]S. Qu, "Zen Magnets." http://zenmagnets.com/ (accessed 22-July-2021), 2021.

[24]B. A. Cipra, "An Introduction to the Ising Model," *The American Mathematical Monthly*, vol. 94, no. 10, pp. 937–959, 1987.

[25]R. Fitzpatrick, "The Ising Model." http://farside.ph.utexas.edu/teaching/329/lectures/node110.html (accessed 06-Jul-2021), 2021.

[26]P. T. Haugen, A. D. P. Smith, and B. F. Edwards, "Normal mode oscillations for the circular and dipolar states of a filled hexagonal magnetic dipole cluster," *Chaos*, 2021.

[27]D. J. Griffiths, "Introduction to electrodynamics," *Introduction to Electrodynamics*, 1989. Cited By :2818.

[28]R. P. Feynman, R. B. Leighton, and M. Sands, *The Feynman lectures on physics, Vol. I: The new millennium edition: mainly mechanics, radiation, and heat; Sec. 52-5, Polar and Axial Vectors*, vol. 1. Basic books, https://www.feynmanlectures.caltech.edu/I_52.html, 2011.

[29]Wikipedia, "Pseudovector." https://en.wikipedia.org/wiki/Pseudovector (accessed 02-August-2021), 2021.

[30]Bilbao Crystallographic Server, "Magnetic Point Group Tables." https://www.cryst.ehu.es/cryst/mpoint.html (accessed 02-August-2021), 2021.